Quantification of Arterial, Venous, and Cerebrospinal Fluid Flow Dynamics by Magnetic Resonance Imaging Under Simulated Micro-Gravity Conditions: A Prospective Cohort Study

Arslan Zahid (arslanz1010@gmail.com)
Emory University School of Medicine https://orcid.org/0000-0002-4586-6751
Bryn Martin
University of Idaho
Stephanie Collins
Georgia Institute of Technology
John N. Oshinski
Emory University
Christopher Ross Ethier
Georgia Institute of Technology

Research

Keywords: Spaceflight-Associated Neuro-Ocular Syndrome, head-down tilt, arterial, venous, cerebrospinal fluid dynamics, simulated microgravity

Posted Date: March 9th, 2020

DOI: https://doi.org/10.21203/rs.3.rs-16448/v1

Version of Record: A version of this preprint was published on February 12th, 2021. See the published version at https://doi.org/10.1186/s12987-021-00238-3.

Abstract

Background: Astronauts undergoing long-duration spaceflight are exposed to numerous health risks, including Spaceflight-Associated Neuro-Ocular Syndrome (SANS), a spectrum of ophthalmic changes that can result in permanent loss of visual acuity. The etiology of SANS is not well understood but is thought to involve changes in cerebrovascular flow dynamics in response to microgravity. There is a paucity of knowledge in this area; in particular, cerebrospinal fluid (CSF) flow dynamics have not been well characterized under microgravity conditions. Our study was designed to determine the effect of simulated microgravity (head-down tilt [HDT]) on cerebrovascular flow dynamics. We hypothesized that under microgravity conditions simulated by HDT, increased pressure in the intracranial space would alter intracranial CSF and venous flow dynamics by causing: 1) venous congestion reflected by increased venous cross-sectional area; and 2) a decrease in cardiac-related CSF flow oscillations.

Methods: In a prospective cohort study, we measured flow in major cerebral arteries, veins, and CSF spaces in fifteen healthy volunteers using phase contrast magnetic resonance (PCMR) before and during 15° HDT.

Results: We found a significant increase in venous cross-sectional area with HDT (p=0.005), indicating venous congestion, along with a decrease in all CSF flow parameters [systolic peak flow (p=0.009), peak-to-peak pulse amplitude (p=0.001), and stroke volume (p=0.10)]. Arterial average flow (p=0.04), systolic peak flow (p=0.04), and peak-to-peak pulse amplitude (p=0.02) all also significantly decreased.

Conclusions: These results collectively demonstrate that acute application of 15° HDT caused a reduction in CSF flow parameters (systolic peak flow and peak-to-peak pulse amplitude), coupled with an increase in venous CSA suggesting increased venous congestion with HDT.

Background

Microgravity has been associated with multiple maladaptive physiological processes. For example, blood volumes and pressures are known to be affected during spaceflight [1]. However, less well understood are alterations to cerebrospinal fluid (CSF) flow and pressures in microgravity. CSF production and its flow characteristics serve as a key component of the physiological homeostasis, immunological protection, and metabolic maintenance of the central nervous system. Perturbations of CSF homeostasis can result in pathological outcomes such as hydrocephalus, which can enlarge the cranial vault and result in developmental deficits, and idiopathic intracranial hypertension (IIH), which often results in headaches, ocular pathologies, and abnormal gait [2-4]. Magnetic resonance imaging (MRI) studies in astronauts before and after spaceflight missions have shown perturbations to the CSF spaces, predominantly after long-duration missions, including narrowing of the central sulcus, upward shift of the brain, and narrowing of the CSF spaces at the vertex [5].

A spaceflight induced condition thought to be related to alterations in CSF flow dynamics is Spaceflight Associated Neuro-ocular Syndrome (SANS), a spectrum of poorly understood neuro-ophthalmological findings documented in a subset of astronauts returning from the International Space Station. Clinical findings of SANS include unilateral and bilateral optic disc edema, globe flattening, choroidal and retinal folds, hyperopic refractive error shifts, and choroidal and nerve fiber layer thickening [6]. Of seven United States astronauts evaluated for SANS after long-duration spaceflight of greater than six months, six developed decreased near field vision with nerve fiber layer thickening; five exhibited optic disc edema, globe flattening, and choroidal folds; and three had nerve fiber layer thickening [6, 7]. Four individuals who underwent postflight lumbar puncture for measurement of CSF pressure exhibited an elevated average opening pressure of 28 cm H_2O up to 12 days after reentry [6, 7]. In addition, postflight surveys of 300 astronauts suggest that inflight loss of both near and distant visual acuity is a significant issue that increases in prevalence with duration of flight, with 29% of short duration and 60% of long duration mission participants reporting some degree of loss in visual acuity [6, 8].

Alterations in CSF dynamics secondary to loss of hydrostatic pressure gradients in microgravity are thought to play a role in SANS. Such alterations may include an overall mild elevation in intracranial pressure (ICP) and/or a loss of normal CSF pressure changes due to postural changes on Earth. Such CSF pressure changes may in turn contribute to the pathophysiology of SANS due to a mismatch between ICP and intraocular pressure (IOP) [8].

The interplay between cerebral blood flow (CBF) and CSF flow is an important driver of ICP, and thus this coupling may influence ICP/IOP mismatch [8]. However, the coupling of CBF and CSF is not well understood in the context of microgravity. Work by Roberts et al. suggests that the upward shift of the brain with tissue crowding at the vertex may compress adjacent venous structures or obstruct

arachnoid granulations along the superior sagittal sinus, causing obstruction of CSF and venous outflow, thereby resulting in an elevation of intracranial pressure [5]. An improved understanding of this complex coupling process would be valuable in its own right, as well as being useful for helping to validate whole-body models that predict SANS pathophysiology and seek to evaluate the effectiveness of countermeasures [8-10].

Head-down tilt (HDT) has been used to simulate microgravity in ground-based studies that seek to quantify changes in arterial and venous flow dynamics. However, prior studies have yielded conflicting results about arterial blood flow dynamics [11, 12] and have not comprehensively studied CSF flow dynamics, which is an important underlying aspect of the “fluids shift” hypothesis for SANS [8].

In this study, we hypothesized that under microgravity conditions simulated by HDT, increased pressure in the intracranial space would alter intracranial CSF and venous flow dynamics by causing: 1) venous congestion reflected by increased venous cross-sectional area; and 2) a decrease in cardiac-related CSF flow oscillations. Our study was designed to analyze the effect of HDT simulated microgravity on cerebrovascular flow dynamics by measuring flow through major arteries, veins, and CSF spaces using phase contrast magnetic resonance (PCMR) before and after acute application of 15° HDT in healthy volunteers.

Materials And Methods

Study Design:

Fifteen healthy subjects participated in this NASA and Emory University IRB-approved study protocol. This study adhered to the tenets of the Declaration of Helsinki. Criteria for inclusion in the study included age ≥18 years, no contraindications to non-contrast MRI, no self-reported cardiovascular or neurological disease, and no current pregnancy. Written informed consent was obtained for all volunteers. All data was anonymized prior to analysis.

Physiological Measurements:

Heart rate was monitored throughout the exam using a peripheral pulse unit applied to the first digit of the volunteer’s left hand. Blood pressure readings were taken prior to the exam, prior to HDT, and after HDT. Blood pressure readings were taken with a MR-safe digital automated sphygmomanometer applied to the bicep while the volunteer was supine.

In-Vivo MRI Measurements:

All volunteers were scanned on a 3 T MRI scanner (Prisma Siemens Medical Systems, Malvern, PA) using a 20-channel head coil. Two-dimensional cine phase-contrast MRI (PCMR) images were acquired in the transverse orientation at the mid-C2 vertebral level using a previously published protocol [13]. Images were acquired with through-plane velocity encoding in the supine position and again after a 30-minute acclimation period at 15° HDT (Fig 1). Forty images were reconstructed for each cardiac cycle using retrospective peripheral pulse unit (PPU) gating. Imaging parameters included a field-of-view (FOV) = 175 x 175 mm, in-plane resolution = 1.1 x 1.1 mm, slice thickness = 5.0 mm, repetition time (TR) = 11 ms, echo time (TE) = 7 ms, flip angle = 30°, and two segments. Two scans were acquired at the mid-C2 location, one with a velocity encoding (VENC) value of 80 cm/s for blood flow and one with a VENC value of 10 cm/s for CSF flow. The 15° HDT was achieved using a custom-made wedge (Fig 1). This scan protocol was performed twice for each volunteer, first while supine, and then in HDT following a 30 minute acclimatization period under HDT (Fig 2).

Figure 1. Volunteer in -15° head-down tilt in the MR scanner. Note that the head (not pictured) was positioned within a radiofrequency coil that required it to be positioned at 0° orientation above the neck.

Figure 2. Schematic of scan protocol showing examples of CSF and blood flow acquisition. Top panels: anatomic image used to identify vessels and other structures. Bottom panels: phase contrast image showing craniocaudal velocities (greyscale). See Figure 3 for identification of colored regions.

To quantify CSF, venous, and arterial flow, regions of interest (ROI) were outlined within the subarachnoid space, the bilateral internal jugular veins, and the bilateral internal carotid and vertebral arteries, respectively (Fig 3). ROIs were drawn manually to approximate the contours of each vessel using FLOW software suite (LUMC, Lieden, The Netherlands) [14, 15]. Each ROI for each of the forty images per scan was visually inspected to ensure quality of the contours. The automatic segmentation feature was applied at each time-step to correctly segment the vessel wall. All ROIs were visually inspected to assure that phase aliasing was not present, and if found, phase unwrapping was applied.

Figure 3. Example of CSF (image 1), arterial (image 2), and venous (image 3) ROIs as seen on an axial view at the mid-C2 vertebral level. Each scan is from a different volunteer. Left greyscale panels: phase contrast image showing craniocaudal velocities (greyscale). Right panels: anatomic image used to identify vessels and other structures. Image 1 structures: subarachnoid space (red). Image 2 structures: internal carotid (red and green) and vertebral arteries (white and blue). Image 3 structures: Internal jugular veins (red and green). Instantaneous flow rates (mL/min) at 40 time points throughout the cardiac cycle were determined in the veins, arteries, and CSF spaces using the ROI area and corresponding average velocity measurements as determined by the FLOW program (Fig 5). The software also provided stroke volumes for each vessel, defined as the net blood volume crossing the measurement plane per cardiac cycle.

We assumed that measured CSF flows should sum to zero over the cardiac cycle due to the oscillatory nature of CSF flow dynamics with approximately zero net flow present in the spinal subarachnoid space [16]. In practice, this was not observed, due to the presence of eddy currents and background phase offsets in the PCMR scan [17]. Therefore, we specified a subject-specific flow rate offset to force the net CSF flow to be zero over each cardiac cycle as has been done in previous studies [18-21]. The average required offset magnitude was 0.22 ± 0.34 mL/s. Similar to previous publications, we computed CSF stroke volume as half of the integral of the absolute value of CSF flow rate over the cardiac cycle. Numerical integration was performed using the trapezoid rule (Fig 4) [22].

Our primary outcome measures were: average flow rate over the cardiac cycle, systolic peak flow rate, peak-to-peak flow pulse amplitude (PtPPA), stroke volume (SV), and cross-sectional area (CSA) for arteries, veins, and the spinal subarachnoid space (Fig 4). These outcome measures were determined from a combination of ROI on the PCMR cine magnitude images (providing CSA) as well as measured velocity through that area.

Statistical Analysis:

SAS version 9.4 and Microsoft Excel were used to conduct all data analyses. Normality for all study parameters was assessed with a Shapiro-Wilk test. All outcome measures apart from venous cross-sectional area passed the Shapiro-Wilk test and were therefore analyzed through parametric methods, namely by paired two-tailed t-tests (supine vs. HDT). The comparisons in these statistical tests were conducted on each individual in a paired manner, comparing before and after HDT rather than a comparison between groups. The statistical significance of the difference in venous cross-sectional area due to HDT was accordingly analyzed through the non-parametric Wilcoxon signed-rank test. Differences were considered significant at p-value < 0.05.

Results

Fifteen healthy subjects (7 males, 8 females; mean age ± SD: 29.5 ± 12.1 yrs.) participated in the study. Vital signs revealed no significant difference between heart rates or systolic and diastolic blood pressure before and after HDT (Table 1), although there was a trend towards higher blood pressures after HDT.

Table 1. Change in vital signs due to HDT (n=15).

Vital Sign	Average Pre-HDT	Average Post-HDT	*p*-value
HR (bpm)	60 ± 9	59 ± 6	.590
SBP (mmHg)	110 ± 14	116 ± 10	.442
DBP (mmHg)	64 ± 12	71 ± 7	.086

Abbreviations: HDT: head-down tilt; HR: heart rate; SBP: systolic blood pressure; DBP: diastolic blood pressure.

Instantaneous flow rates (mL/min) at 40 time points throughout the cardiac cycle were determined in the veins, arteries, and CSF space using the ROI area and corresponding average velocity measurements as determined by the FLOW program (Figs 4-5).

Figure 4. Representative CSF flow rate vs. time over a cardiac cycle, showing the definitions of flow and stroke volume parameters. Note that negative flow rates present during systole are in the craniocaudal direction. The pulse was monitored by a peripheral pulse unit applied to the first digit of the volunteer's hand, and the local systolic flow peak occurs earlier at the vessels of the neck than at the first digit, explaining the location of the systolic peak in this figure. Time zero of the cardiac cycle in this figure represents the detected pulse peak at the finger.

Figure 5. Representative arterial and venous flow rates vs. time over a cardiac cycle for a single subject for the right internal carotid artery and the right internal jugular vein. Negative values indicate flow towards the heart. The explanation for the late location of the systolic peak in this figure is the same as for Figure 4.

All venous blood flow parameters showed a trend towards increased magnitude during HDT, but none of these changes were significant other than an increase in the internal jugular vein cross-sectional area (Table 2, Figure 6). All arterial blood flow parameters decreased in HDT, with changes in average blood flow rate, systolic peak flow rate, and PtPPA all reaching statistical significance (Table 2). Finally, all measured parameters for CSF flow decreased from supine to HDT postures, with statistically significant decreases observed in systolic peak flow rate and PtPPA. (Table 2, Figure 7, Figure 8). There was also a decrease in SV, but it did not reach statistical significance.

Table 2. Changes in cerebrovascular flow dynamics from baseline (supine position) to HDT (n=15 subjects).

	Arterial blood flow				Venous blood flow				CSF flow			
	Baseline	HDT	%Δ	*p*-value	Baseline	HDT	%Δ	*p*-value	Baseline	HDT	%Δ	*p*-value
Average flow (mL/min)	867 ± 172	819 ± 177	-6%	0.040*	-551 ± 214	-572 ± 157	+4%	0.30	-	-	-	-
Systolic Peak flow (mL/min)	570 ± 108	522 ± 102	-8%	0.040*	-474 ± 384	-576 ± 222	+22%	0.24	-234 ± 84	-186 ± 66	-21%	0.0088*
PtPPA (mL/min)	510 ± 126	450 ± 126	-12%	0.020*	-456 ± 276	-486 ± 264	+7%	0.24	372 ± 108	312 ± 102	-16%	0.00098*
SV (mL/cardiac cycle)	15 ± 2.8	14 ± 3.4	-7%	0.43	10 ± 4.6	10 ± 2.4	0%	0.99	0.77 ± 0.20	.68 ± .16	-12%	0.10
CSA (mm^2)	41 ± 7.6	43 ± 8.8	+5%	0.32	82 ± 31	94 ± 40	+15%	0.0050*	-	-	-	-

Abbreviations: HDT: head-down tilt; CSF: cerebrospinal fluid; PtPPA: peak-to-peak pulse amplitude; SV: stroke volume; CSA: cross-sectional area. Asterisks indicate statistical significance.

Figure 6. Changes in venous cross sectional area (CSA) from supine to head-down tilt (HDT). Left panel: scatter plot of individual internal jugular vein CSAs, with two internal jugular veins plotted per volunteer, connected from supine to HDT. Right panel: five-number summary box plot of the same internal jugular vein CSAs at supine and HDT.

Figure 7. Changes in cerebrospinal fluid (CSF) peak-to-peak pulse amplitude (PtPPA) from supine to head-down tilt (HDT). Left panel: scatter plot of each volunteer's CSF PtPPA connected from supine to HDT. Right panel: five-number summary box plot of the same CSF PtPPAs at supine and HDT.

Figure 8. Changes in cerebrospinal fluid (CSF) systolic peak flow rate from supine to head-down tilt (HDT). Left panel: scatter plot of each volunteer's CSF systolic peak flow connected from supine to HDT. Right panel: five-number summary box plot of the same CSF systolic peak flow rates at supine and HDT. Negative values indicate CSF flow away from the head.

Discussion

The hypothesis of our study was that microgravity, as simulated through acute application of 15° HDT, would increase intracranial pressure and alter cerebral blood and spinal CSF flow by causing: 1) venous congestion reflected by increased vein cross-sectional area; and 2) a decrease in CSF flow oscillations. As hypothesized, HDT did significantly decrease CSF flow oscillations at the mid-C2 vertebral level as manifested by reduced systolic peak flow rate and PtPPA. A significant increase in venous cross-sectional area was also observed, which is indicative of venous congestion. An unexpected finding of our study was that HDT significantly decreased arterial average flow rate, systolic peak flow rate, and PtPPA.

Spaceflight has been hypothesized to cause a headward shift of CSF and our results, given the physiology of CSF production and flow, support this hypothesis. Prior studies have examined cerebral flow dynamics under HDT. Marshall-Goebel et al., using 9 healthy male volunteers, found a decrease in both arterial and venous flow rate parameters as well as an increase in venous cross-sectional area (CSA) from baseline to HDT (62 mm^2 to 97 mm^2), suggestive of venous congestion [11]. Ishida et al., using 15 healthy volunteers, found increases in venous CSA (36 mm^2 to 54 mm^2), decreases in arterial inflow, increases in venous outflow, and no significant changes in CSF stroke volume or systolic velocity [12]. These observed changes in venous CSA under ground-based HDT are consistent with ultrasound studies performed during spaceflight that demonstrate comparable increases in venous CSA in subjects exposed to microgravity [23, 24]. These prior studies collectively corroborate our findings of increased venous CSA. Our study also reproduces the decrease in arterial flow parameters seen in these studies. Finally, we observe a decrease in CSF flow oscillations not examined in these prior studies.

To help understand our CSF results, it is useful to recall several aspects of CSF physiology under normal gravity conditions. CSF is produced in the choroid plexus of the brain's ventricles and slowly circulates into the spinal and cranial subarachnoid spaces [25]. It is then absorbed into the venous system via arachnoid granulations, primarily near the dural venous sinus [25]. An increase in venous pressure of only a few mmHg can alter the pressure gradient across the arachnoid granulations, leading to reduced CSF absorption [8]. Our study did not directly measure the location of the CSF space center of gravity and therefore cannot conclude that a fluid shift of CSF occurred. However, any shift in CSF center of gravity towards the head would potentially have a downstream impact on CSF flow amplitude by altering intracranial compliance.

Beyond production and absorption, CSF homeostasis is directly coupled to venous flow dynamics, which is evident by considering data from respiration studies. During inspiration, the chest wall expands and creates negative intrathoracic pressure, which allows for the lungs to fill and also causes venous outflow from the head [25, 26]. CSF flow has been observed to be coupled with these intracranial venous changes, with inspiration yielding net CSF flow towards the head while expiration leads to pronounced downward CSF flow [25, 26]. In other words, physiological maneuvers that bring venous blood to the upper body push CSF fluid back into the head, and those that relax venous congestion in the upper body allow for CSF to flow down the spine and away from the head.

SANS may involve perturbations to CSF flow given the pathological findings of optic disc edema, globe flattening, and decreased visual acuity that are also present in Earth-bound conditions of CSF imbalance such as idiopathic intracranial hypertension [4, 6]. CSF dynamics can be altered by changes in production, flow, or reabsorption. The former and latter occur slowly, and thus are relatively unimportant in the setting of an acute study, such as we have conducted. This leaves changes in arterial flow and the aforementioned physiological coupling with venous flow as plausible explanations for our observed CSF changes.

As shown in our study, heart rate and blood pressure do not significantly change from baseline to HDT, but there are significant decreases in arterial flow parameters. Most notably, a decrease in arterial flow could drive decreased CSF flow pulsation, which was observed. In addition, the cross-sectional area of the veins significantly increased, which indicate venous congestion in the neck veins. This venous congestion could be responsible for the CSF outflow obstruction that is implied by the observed decrease in CSF flow parameters in our study. This pathophysiological connection is supported by prior HDT MRI studies that consistently demonstrate that simulated microgravity causes venous congestion as well as decreased arterial flow, although our study is the first to connect those parameters with directly observed changes in CSF flow dynamics.

Our results however do not provide evidence for whether arterial flow or venous congestion is the primary driver for our observed CSF changes since we were unable to control each parameter independently. Furthermore, the argument for venous congestion in our results is moderated by the fact that venous blood flow itself did not significantly change from baseline to HDT. Moreover, given our limited sample size, we can at best report this as an association and cannot directly linearly tie increased in venous CSA with decreases in CSF flow oscillations. In support of our findings, however, significant jugular venous blood flow stasis has been reported in International Space Station crew members during long-duration spaceflight missions with significant increases in venous jugular CSA noted when comparing ultrasound-based preflight measurements to measurements taken during spaceflight [27]. Notably, this increase in CSA was associated with stagnant blood flow, and these findings were clinically significant when one crew member was found to have developed an occlusive IJV thrombus [27].

Apart from the pathophysiological alterations suggested by the measurements in our study, these parameters are additionally useful inputs for models seeking to simulate volume and pressure alterations in the head and eye in microgravitational settings. Prior

studies have relied on blood and aqueous humor dynamics as inputs to improve and extend these models, and we anticipate that these results will be similarly useful for models seeking to replicate the pathophysiology of SANS [9].

A primary limitation of our study was the use of HDT as a proxy for microgravity. Although HDT has been utilized in many previous studies to simulate microgravity, it cannot reproduce other spaceflight-related nongravitational factors such as alterations to fluid and electrolyte balance, cardiovascular and pulmonary function, and metabolism, and so the generalizability of any findings to spaceflight has these inherent limitations [28, 29]. An additional limitation includes the duration of the study. As previously mentioned, ocular symptoms in astronauts increase in prevalence with duration of spaceflight, and a 30-minute HDT analog captures only acute changes. Moreover, an ideal angle for HDT has not been established, with a range of angles from 6° to 15° being used. The 15° angle used in our study may have been too steep and we cannot ensure that our CSF findings would have been replicated with a lower degree of HDT. A study using a 15° HDT protocol to assess venous jugular blood flow before, during, and after spaceflight on International Space Station crew members demonstrated that venous CSA changes increased from sitting to supine to HDT with a similar magnitude of change between those positions preflight and postflight, although HDT in both of those settings overestimated increases in venous CSA found in-flight [27]. However, our venous and arterial changes from baseline to 15° HDT are corroborated by prior studies at these lower degrees of HDT, which lends support to the validity of our CSF findings at 15° [11, 12, 30].

Other limitations included the fact that our recorded venous outflow did not account for the entirety of arterial inflow, indicating missing venous collateral changes in flow. Similarly, the internal carotid and vertebral arteries do not account for the entirety of arterial inflow to the head, and so the observed decrease in arterial inflow seen with HDT could also be due to diversion of arterial blood flow to other vessels. An alternative explanation could be due alterations in carbon dioxide levels due to anxiety and increased respiration while in HDT: Yiallourou et al. previously had similar findings in changes in intracranial flow following alterations to carbon dioxide levels with the application of continuous positive airway pressure [31]. An additional limitation was that, due to time constraints, we did not repeat the scan protocol afterwards again in the supine position to assess for a return to baseline.

In terms of limitations in statistical analysis, we chose not to apply a Bonferonni correction for multiple comparisons (due to the multiple parameters in our study) so as to not make a type II error more likely. However, a lack of correction for multiple comparisons does increase the likelihood of a type I error. As a result, chance associations may exist, and our positive findings should to be replicated. A final limitation includes the lack of well-defined minimal clinically important differences (MCIDs) in our flow parameters with respect to SANS.

Future studies should compare arterial, venous, and CSF flow parameters in astronauts pre- and post-flight, particularly in those experiencing SANS symptoms in order to generate MCIDs. Non-invasive measurements of these flow parameters in astronauts during spaceflight would also be ideal if permitted by technology. In addition, comparisons of HDT parameters with imaging from astronauts would help validate HDT as a tool for further investigation of physiological changes to the head in microgravity, which would be critical to justify future studies examining specific populations of interest such as women, minorities, various age groups, or even children to create more individualized risk profiles and predictive models.

In conclusion, we have demonstrated that acute application of 15° HDT simulated microgravity is associated with alterations in intracranial blood flow and spinal CSF flow dynamics. HDT caused a reduction in CSF flow parameters measuring peak systolic flow and peak-to-peak pulse amplitude which were coupled with an increase in venous CSA suggesting increased venous congestion with HDT. Decreased arterial inflow seen in previous studies with HDT was confirmed in this study.

Declarations

Ethics approval and consent to participate

This study was approved by both the NASA and Emory University IRBs.

Consent for publication

Not applicable

Availability of data and materials

The datasets used and analyzed during this study are available from the corresponding author on reasonable request.

Competing interests

The authors declare that they have no competing interests.

Funding

This work was funded by Georgia CTSA Grants TL1TR002382 and UL1TR002378, NASA grant NNX16AT06G, and the Georgia Research Alliance (CRE).

References

1. Norsk, P., et al., *Fluid shifts, vasodilatation and ambulatory blood pressure reduction during long duration spaceflight.* J Physiol, 2015. **593**(3): p. 573-84.
2. Yamada, S. and E. Kelly, *Cerebrospinal Fluid Dynamics and the Pathophysiology of Hydrocephalus: New Concepts.* Semin Ultrasound CT MR, 2016. **37**(2): p. 84-91.
3. Stevens, S.M., et al., *Idiopathic intracranial hypertension: Contemporary review and implications for the otolaryngologist.* Laryngoscope, 2018. **128**(1): p. 248-256.
4. Hu, R., et al., *Cerebrospinal Fluid Pressure Reduction Results in Dynamic Changes in Optic Nerve Angle on Magnetic Resonance Imaging.* J Neuroophthalmol, 2019. **39**(1): p. 35-40.
5. Roberts, D.R., et al., *Effects of Spaceflight on Astronaut Brain Structure as Indicated on MRI.* N Engl J Med, 2017. **377**(18): p. 1746-1753.
6. Lee, A.G., et al., *Space Flight-Associated Neuro-ocular Syndrome.* JAMA Ophthalmol, 2017. **135**(9): p. 992-994.
7. Mader, T.H., et al., *Optic disc edema in an astronaut after repeat long-duration space flight.* J Neuroophthalmol, 2013. **33**(3): p. 249-55.
8. Zhang, L.F. and A.R. Hargens, *Spaceflight-Induced Intracranial Hypertension and Visual Impairment: Pathophysiology and Countermeasures.* Physiol Rev, 2018. **98**(1): p. 59-87.
9. Nelson, E.S., et al., *The impact of ocular hemodynamics and intracranial pressure on intraocular pressure during acute gravitational changes.* J Appl Physiol (1985), 2017. **123**(2): p. 352-363.
10. Feola, A.J., et al., *Finite Element Modeling of Factors Influencing Optic Nerve Head Deformation Due to Intracranial Pressure.* Invest Ophthalmol Vis Sci, 2016. **57**(4): p. 1901-11.
11. Marshall-Goebel, K., et al., *Effects of short-term exposure to head-down tilt on cerebral hemodynamics: a prospective evaluation of a spaceflight analog using phase-contrast MRI.* J Appl Physiol (1985), 2016. **120**(12): p. 1466-73.
12. Ishida, S., et al., *MRI-based assessment of acute effect of head-down tilt position on intracranial hemodynamics and hydrodynamics.* J Magn Reson Imaging, 2018. **47**(2): p. 565-571.
13. Lawrence, B.J., et al., *Cardiac-Related Spinal Cord Tissue Motion at the Foramen Magnum is Increased in Patients with Type I Chiari Malformation and Decreases Postdecompression Surgery.* World Neurosurg, 2018. **116**: p. e298-e307.
14. van der Geest, R.J., et al., *Automated measurement of volume flow in the ascending aorta using MR velocity maps: evaluation of inter- and intraobserver variability in healthy volunteers.* J Comput Assist Tomogr, 1998. **22**(6): p. 904-11.
15. van 't Klooster, R., et al., *Automatic lumen and outer wall segmentation of the carotid artery using deformable three-dimensional models in MR angiography and vessel wall images.* J Magn Reson Imaging, 2012. **35**(1): p. 156-65.
16. Sanchez, A.L., et al., *On the bulk motion of the cerebrospinal fluid in the spinal canal.* Journal of Fluid Mechanics, 2018. **841**: p. 203-227.
17. Yiallourou, T.I., et al., *Comparison of 4D phase-contrast MRI flow measurements to computational fluid dynamics simulations of cerebrospinal fluid motion in the cervical spine.* PLoS One, 2012. **7(12)**: p. e52284.
18. Sass, L.R., et al., *A 3D suject-specific model of the spinal subarachnoid space with anatomically realistic ventral and dorsal spinal cord nerve rootlets Fluid Barriers CNS* 2017. **14(1)**: p. 36.
19. Quigley, M.F., et al., *Cerebrospinal fluid flow in foramen magnum: temporal and spatial patterns at MR imaging in volunteers and in patients with Chiari I malformation.* Radiology, 2004. **232**(1): p. 229-36.

20. Heidari Pahlavian, S., et al., *Accuracy of 4D Flow Measurement of Cerebrospinal Fluid Dynamics in the Cervical Spine: An In Vitro Verification Against Numerical Simulation. .* Ann Biomed Eng, 2016. **44(11)**: p. 3202-3214.
21. Alperin, N., et al., *Hemodynamically independent analysis of cerebrospinal fluid and brain motion observed with dynamic phase contrast MRI* Magnetic Resonance in Medicine, 1996. **35(5)**: p. 741-754.
22. Alperin, N., et al. , *Magnetic resonance imaging measures of posterior cranial fossa morphology and cerebrospinal fluid physiology in Chiari malformation type I.* Neurosurgery, 2014. **75(5)**: p. 515-22.
23. Herault, S., et al., *Cardiac, arterial and venous adaptation to weightlessness during 6-month MIR spaceflights with and without thigh cuffs (bracelets).* Eur J Appl Physiol, 2000. **81**(5): p. 384-90.
24. Arbeille, P., et al., *Adaptation of the left heart, cerebral and femoral arteries, and jugular and femoral veins during short- and long-term head-down tilt and spaceflights.* Eur J Appl Physiol, 2001. **86**(2): p. 157-68.
25. Dreha-Kulaczewski, S., et al., *Inspiration is the major regulator of human CSF flow.* J Neurosci, 2015. **35**(6): p. 2485-91.
26. Dreha-Kulaczewski, S., et al., *Respiration and the watershed of spinal CSF flow in humans.* Sci Rep, 2018. **8**(1): p. 5594.
27. Marshall-Goebel, K., et al., *Assessment of Jugular Venous Blood Flow Stasis and Thrombosis During Spaceflight.* JAMA Netw Open, 2019. **2**(11): p. e1915011.
28. Watenpaugh, D.E., *Analogs of microgravity: head-down tilt and water immersion.* J Appl Physiol (1985), 2016. **120**(8): p. 904-14.
29. Hargens, A.R. and L. Vico, *Long-duration bed rest as an analog to microgravity.* J Appl Physiol (1985), 2016. **120**(8): p. 891-903.
30. Strangman, G.E., et al., *Increased cerebral blood volume pulsatility during head-down tilt with elevated carbon dioxide: the SPACECOT Study.* J Appl Physiol (1985), 2017. **123**(1): p. 62-70.
31. Yiallourou, T.I., et al., *Continuous positive airway pressure alters cranial blood flow and cerebrospinal fluid dynamics at the craniovertebral junction.* Interdisciplinary Neurosurgery, 2015. **2**(3): p. 152-159.

Figures

Figure 1

Volunteer in -15° head-down tilt in the MR scanner. Note that the head (not pictured) was positioned within a radiofrequency coil that required it to be positioned at 0° orientation above the neck.

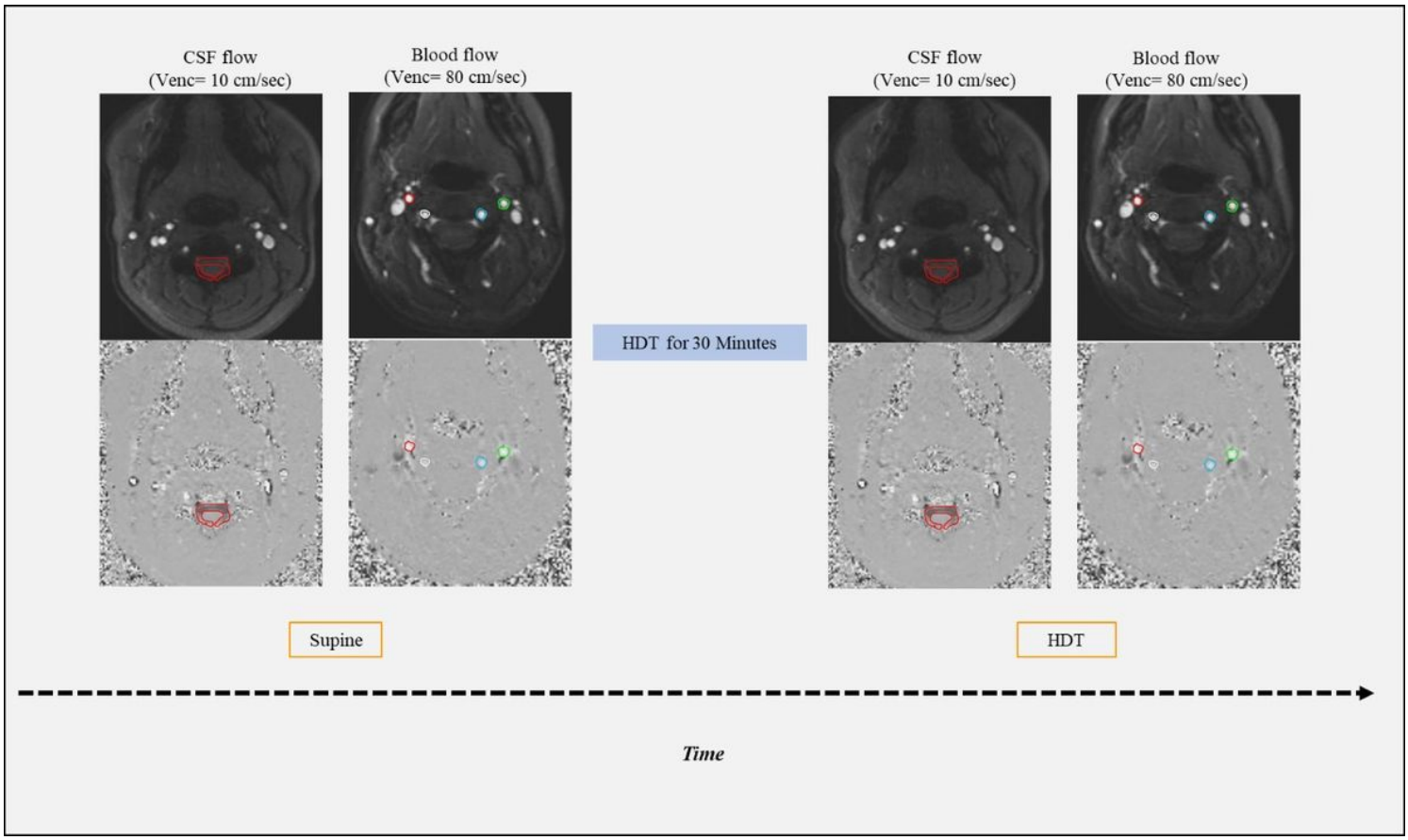

Figure 2

Schematic of scan protocol showing examples of CSF and blood flow acquisition. Top panels: anatomic image used to identify vessels and other structures. Bottom panels: phase contrast image showing craniocaudal velocities (greyscale). See Figure 3 for identification of colored regions.

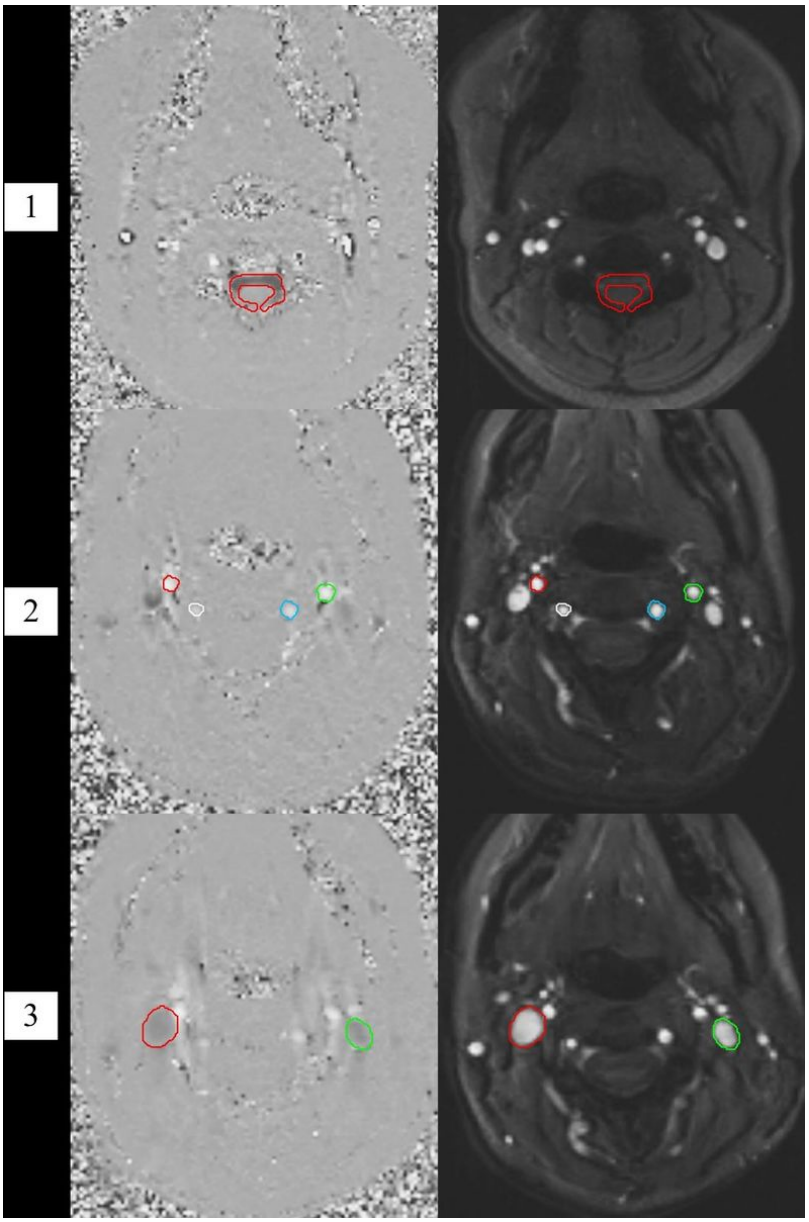

Figure 3

Example of CSF (image 1), arterial (image 2), and venous (image 3) ROIs as seen on an axial view at the mid-C2 vertebral level. Each scan is from a different volunteer. Left greyscale panels: phase contrast image showing craniocaudal velocities (greyscale). Right panels: anatomic image used to identify vessels and other structures. Image 1 structures: subarachnoid space (red). Image 2 structures: internal carotid (red and green) and vertebral arteries (white and blue). Image 3 structures: Internal jugular veins (red and green). Instantaneous flow rates (mL/min) at 40 time points throughout the cardiac cycle were determined in the veins, arteries, and CSF spaces using the ROI area and corresponding average

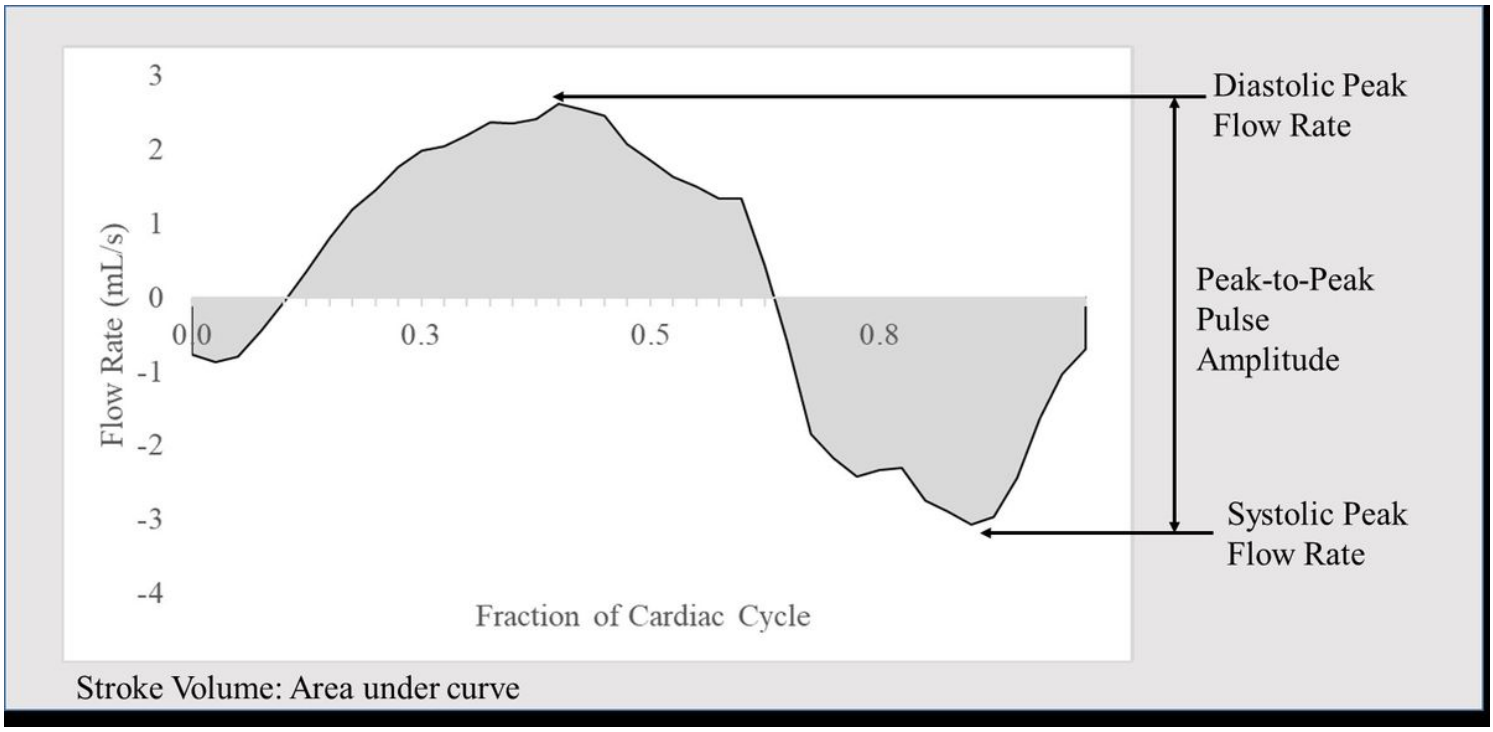

Figure 4

Representative CSF flow rate vs. time over a cardiac cycle, showing the definitions of flow and stroke volume parameters. Note that negative flow rates present during systole are in the craniocaudal direction. The pulse was monitored by a peripheral pulse unit applied to the first digit of the volunteer's hand, and the local systolic flow peak occurs earlier at the vessels of the neck than at the first digit, explaining the location of the systolic peak in this figure. Time zero of the cardiac cycle in this figure represents the detected pulse peak at the finger.

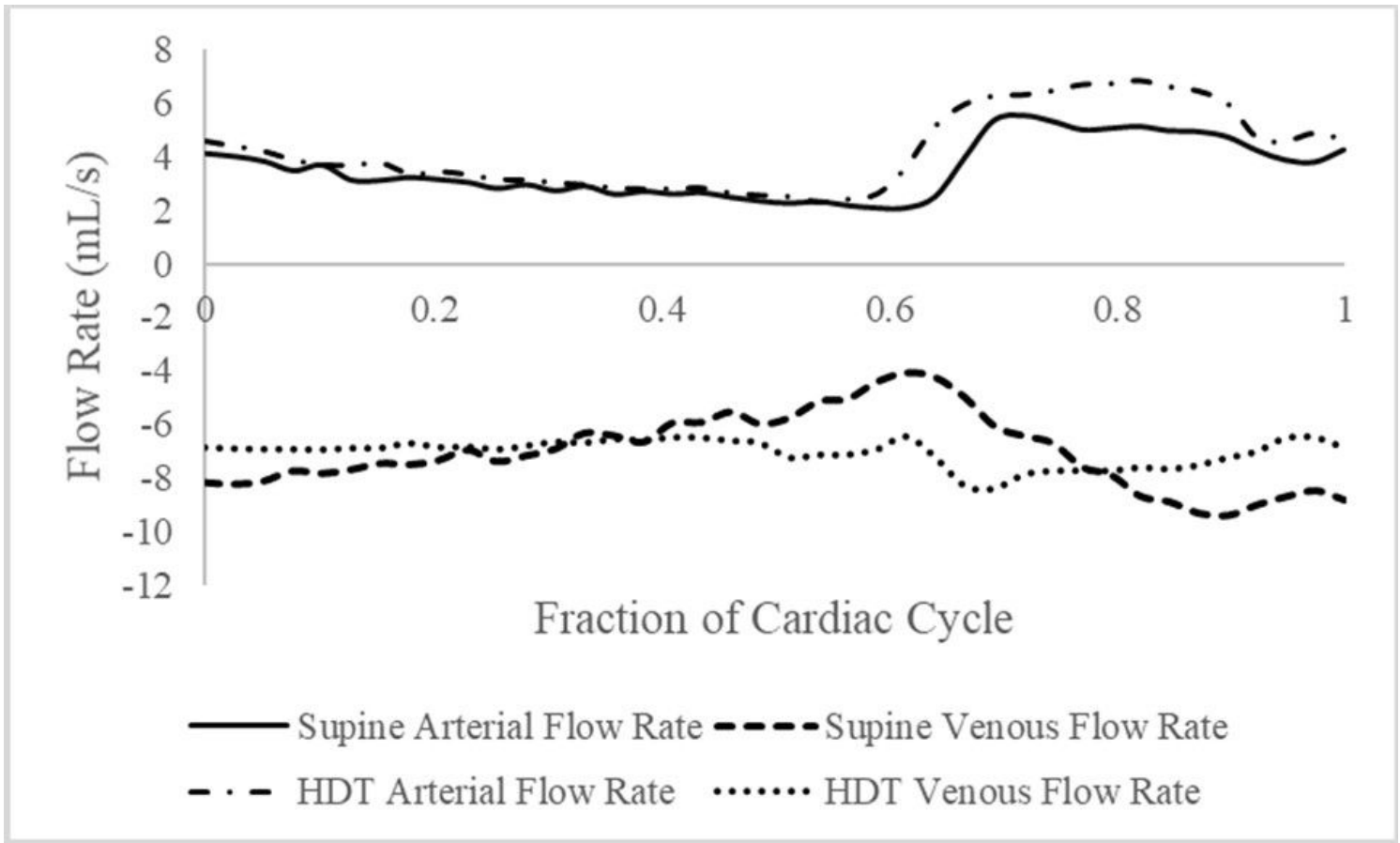

Figure 5

Representative arterial and venous flow rates vs. time over a cardiac cycle for a single subject for the right internal carotid artery and the right internal jugular vein. Negative values indicate flow towards the heart. The explanation for the late location of the systolic peak in this figure is the same as for Figure 4.

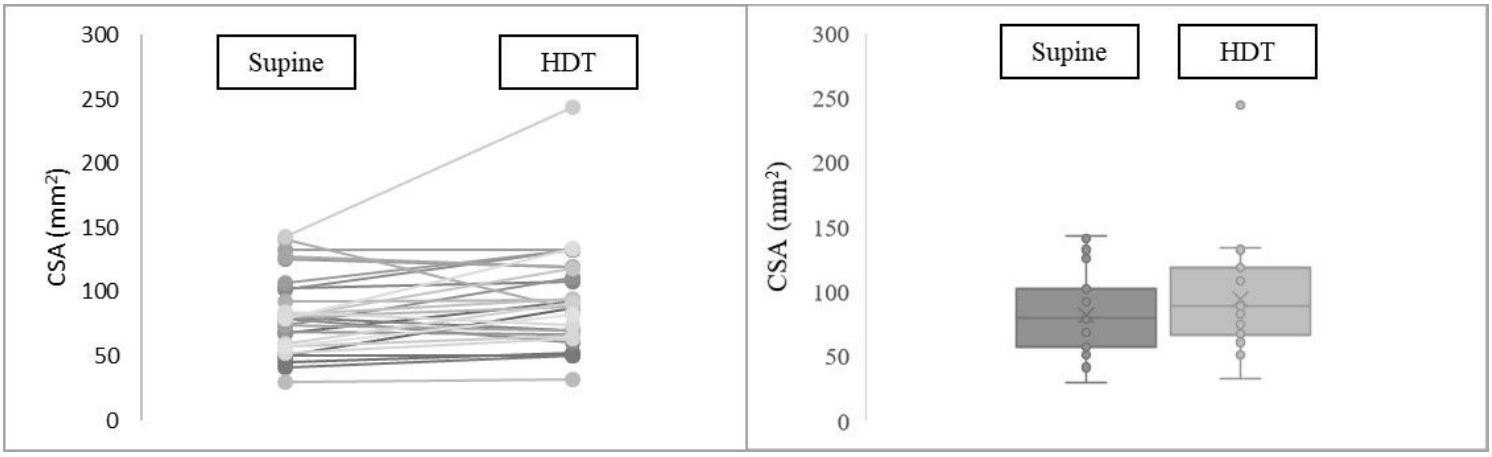

Figure 6

Changes in venous cross sectional area (CSA) from supine to head-down tilt (HDT). Left panel: scatter plot of individual internal jugular vein CSAs, with two internal jugular veins plotted per volunteer, connected from supine to HDT. Right panel: five-number summary box plot of the same internal jugular vein CSAs at supine and HDT.

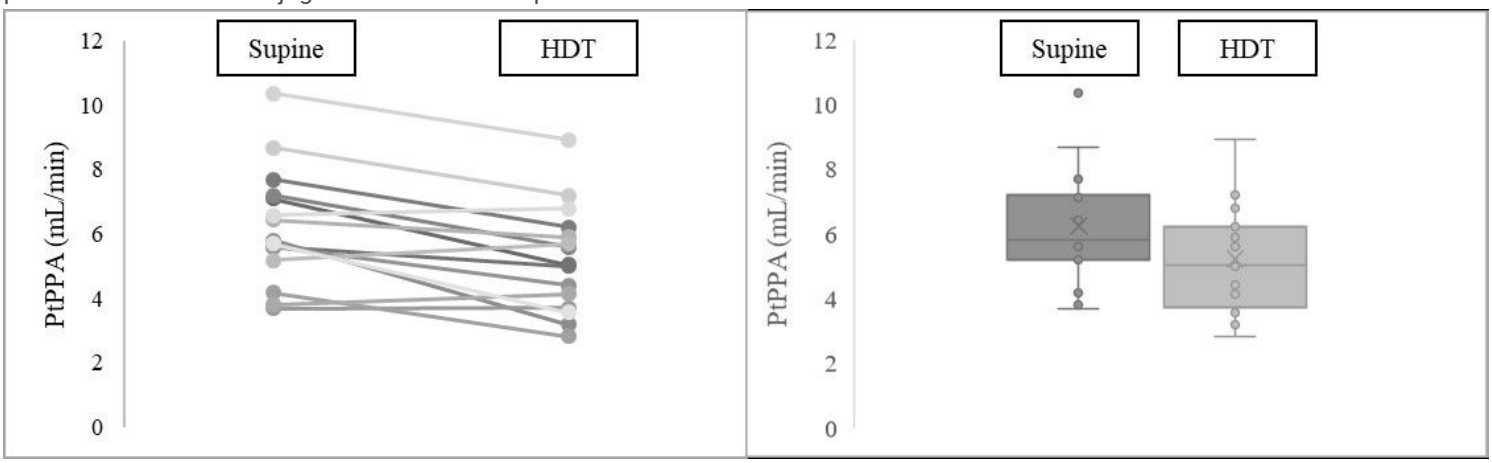

Figure 7

Changes in cerebrospinal fluid (CSF) peak-to-peak pulse amplitude (PtPPA) from supine to head-down tilt (HDT). Left panel: scatter plot of each volunteer's CSF PtPPA connected from supine to HDT. Right panel: five-number summary box plot of the same CSF PtPPAs at supine and HDT.

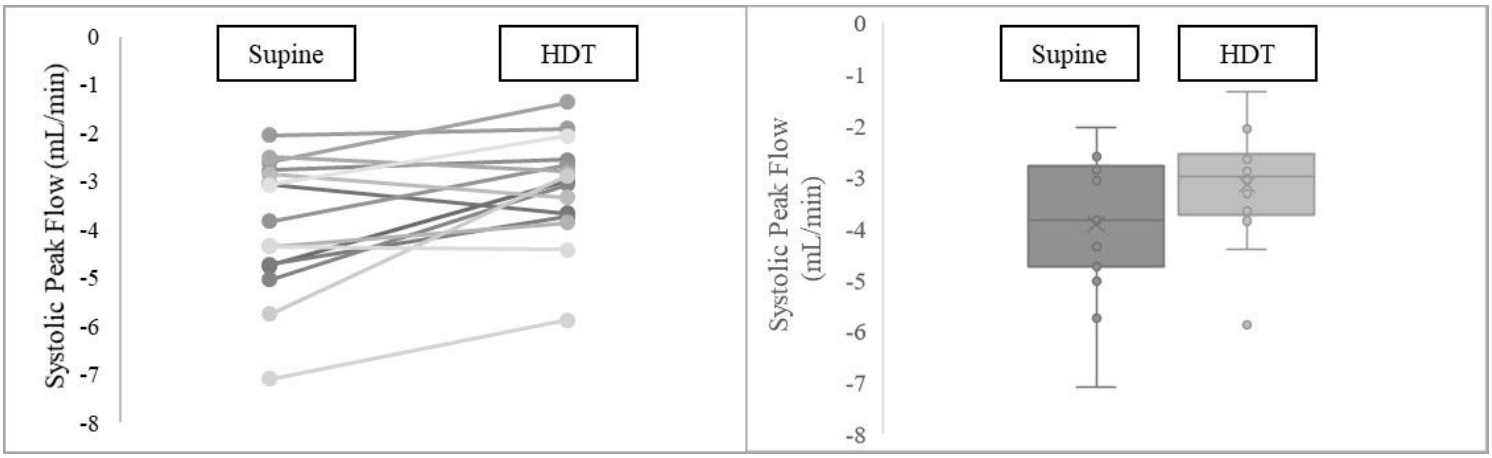

Figure 8

Changes in cerebrospinal fluid (CSF) systolic peak flow rate from supine to head-down tilt (HDT). Left panel: scatter plot of each volunteer's CSF systolic peak flow connected from supine to HDT. Right panel: five-number summary box plot of the same CSF systolic peak flow rates at supine and HDT. Negative values indicate CSF flow away from the head.